Formic Acid Dehydrogenation | Hot Paper

DOI: 10.1002/anie.201405360

Hydrogen from Formic Acid through Its Selective Disproportionation over Sodium Germanate—A Non-Transition-Metal Catalysis System**

Ruth I. J. Amos, Falk Heinroth, Bun Chan,* Sisi Zheng, Brian S. Haynes, Christopher J. Easton, Anthony F. Masters,* Leo Radom,* and Thomas Maschmeyer**

Abstract: *A robust catalyst for the selective dehydrogenation of formic acid to liberate hydrogen gas has been designed computationally, and also successfully demonstrated experimentally. This is the first such catalyst not based on transition metals, and it exhibits very encouraging performance. It represents an important step towards the use of renewable formic acid as a hydrogen-storage and transport vector in fuel and energy applications.*

One of the major challenges of the 21st century is to ensure a sufficient and sustainable supply of energy. The availability of fossil fuels is limited and their use is problematic in terms of greenhouse gas emissions. It is therefore highly desirable to find replacement technologies. In this regard, hydrogen, for example, for fuel cells or direct combustion, has been proposed as a clean energy alternative that can be generated from a range of renewable energy inputs. However, many impediments still need to be overcome prior to its widespread use, one of the major difficulties being identification of improved methods for hydrogen transport.[1]

In this context, formic acid represents a possible medium, not only for the storage of H_2 but also for H_2 transport, since formic acid is renewable,[2] liquid, easily stored and handled, not flammable, and nontoxic and has a relatively high energy density.[3] The possible breakdown pathways of formic acid include dehydrogenation, producing H_2 plus CO_2 [Eq. (1)], and dehydration, yielding H_2O plus CO [Eq. (2)].

$$HCOOH \rightarrow H_2 + CO_2 \quad (1)$$

$$HCOOH \rightarrow H_2O + CO \quad (2)$$

Renewable formic acid has a small carbon footprint because the carbon dioxide released during its conversion to hydrogen is consumed during its formation.[4–6] A suitable catalyst for the breakdown of formic acid for use in fuel applications would need to be selective for dehydrogenation as well as being robust and inexpensive.

Silicates, such as Pyrex, porcelain, and etched silica, have been found to catalyze the decomposition of formic acid, producing low levels of hydrogen.[7] Glassy germanates have also been shown to break down formic acid at high temperatures. However, the major product in this case is carbon monoxide.[8] It is well known that silicalite-1 (particularly high-defect samples) quite effectively dehydrates formic acid, producing water and carbon monoxide.[9]

Studies with transition-metal-oxide catalysts have shown that basic catalysts dehydrogenate formic acid, while undesirable dehydration predominates with acidic catalysts.[10] Within this context, the present study investigates the acidity tuning of solid non-transition-metal catalysts for the selective dehydrogenation of formic acid, using both theoretical and experimental approaches. We have approached acidity tuning in two ways—one is to replace silicon atoms with the more basic germanium, while the other is to replace the acidic protons in the catalyst with sodium ions.

We have used ab initio quantum chemical computations to inform and direct our experimental work. To answer the questions that we wish to address, the calculations need only to be qualitatively descriptive, obviating resource-intensive requirements for a fully quantitative treatment. This is the basis for our choice of models for the larger silicalite-1 and germanate structures (see Figure 1). The crystal structure of sodium germanate is complex, containing both octahedral and tetrahedral environments.[11] Accordingly, we used small octahedral and tetrahedral germanate structures as computational models (Figure 1, structures **a**–**d**). Calculations for the germanate structures were performed at the M06-2X/6-311+G(3df,2p)//B3-LYP/6-31+G(d,p) level,[12] using the Gaussian 09 program.[13]

The all-silica structure of interest is silicalite-1, which has an MFI framework.[14,15] There has been some discussion in the literature as to which model size is most appropriate for

[*] Dr. R. I. J. Amos, Dr. F. Heinroth, Dr. B. Chan, Prof. A. F. Masters, Prof. L. Radom, Prof. T. Maschmeyer
School of Chemistry, The University of Sydney
Sydney, NSW 2006 (Australia)
E-mail: ruth.amos@sydney.edu.au
bun.chan@sydney.edu.au
anthony.masters@sydney.edu.au
leo.radom@sydney.edu.au
thomas.maschmeyer@sydney.edu.au
Dr. R. I. J. Amos, Prof. C. J. Easton
CSIRO Energy Transformed Cluster on Biofuels
and Research School of Chemistry, Australian National University
Canberra, ACT 0200 (Australia)
Dr. R. I. J. Amos, Dr. B. Chan, Prof. C. J. Easton, Prof. L. Radom
ARC Centre of Excellence for Free Radical Chemistry and Biotechnology (Australia)
S. Zheng, Prof. B. S. Haynes
School of Chemical and Biomolecular Engineering
The University of Sydney, Sydney, NSW 2006 (Australia)

[**] We gratefully acknowledge funding (to C.J.E., T.M., A.M., and L.R.) from the Australian Research Council (ARC), funding (to R.I.J.A. and C.J.E) from the CSIRO, and generous grants of computer time (to L.R.) from the National Computational Infrastructure (NCI) National Facility and Intersect Australia Ltd.

Supporting information for this article is available on the WWW under http://dx.doi.org/10.1002/anie.201405360.

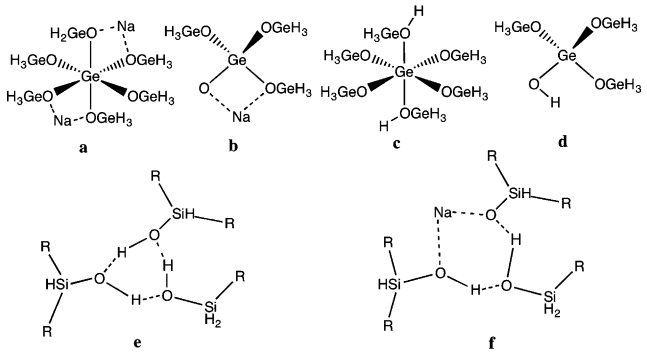

Figure 1. Structures of catalyst models used for the calculations: sodiated octahedral and tetrahedral germanate (**a** and **b**) and protonated octahedral and tetrahedral germanate (**c** and **d**) (calculations were repeated on structures **b** and **d** with each germanium replaced by a silicon atom), and the active site from protonated and sodiated silicalite-1 (**e** and **f**) (calculations repeated on structure **e**) with each silicon atom replaced by a germanium atom). The full silicalite-1 catalyst models can be viewed in the Supporting Information.

particular zeolite frameworks, with some computational studies showing that larger models are necessary for accuracy in calculations,[16] and others finding that calculations on models with four tetrahedral atoms (4T) give results that are very similar to the larger 28T models.[17] It would thus seem that the sensitivity to model size is system dependent. Our calculations involving silicalite-1 showed that a somewhat larger model is required in the present case, as smaller models give rise to the formation of additional hydrogen bonds in the structure, which artificially distort the computational results.

For the H-silicalite-1, therefore, a model representing the cavities of the MFI structure[14,15] was constructed by initially extracting a 28T cluster from the literature crystal structure.[18] The reactivity of silicalite-1 is believed to be associated with silanol defects.[19–21] Hence, such a defect was introduced into the silicalite-1 framework by removing a silicon atom and adding hydrogen atoms to the terminal oxygen atoms thus generated (Figure 1, structures **e** and **f**). Dangling bonds were saturated with hydrogen atoms; their locations were obtained through optimizations with the PM6 semiempirical procedure, keeping the positions of the heavy atoms frozen. In subsequent calculations, the terminal hydrogen atoms were constrained in space to avoid unrealistic distortions of the model during the optimization procedure. For the ONIOM[22] calculations, the clusters were partitioned into two layers, with atoms corresponding to the silicalite-1 defect belonging to the high-level layer. Geometry optimizations were carried out at the ONIOM(B3-LYP/6-31+G(d,p):PM6) level, where the high-level atoms were optimized using B3-LYP/6-31+G(d,p) and the low-level atoms were optimized using the PM6 semiempirical procedure. For the germanium MFI structure, the bond lengths were increased by extending the bonds to the terminal hydrogen atoms and then reoptimizing the structure using ONIOM(B3-LYP/6-31+G(d,p):PM6) (see the Supporting Information for details). Improved energies for all structures were obtained through calculations at the M06-2X/6-311+G(3df,2p) level.

Gibbs free energy corrections to 298 K and 1 atm, derived from the B3-LYP/6-31+G(d,p) calculations for the germanate structures and the ONIOM(B3-LYP/6-31+G(d,p):PM6) calculations for the MFI structures, were incorporated into the total energies. Literature scaling factors[23] were used in the evaluation of the Gibbs free energy corrections.

The general reaction pathway involves the initial formation of a complex of formic acid with the catalyst site (formic acid···catalyst), a concerted transition structure (TS), and a complex between the products and the catalyst (product···catalyst), consistent with previous studies of zeolite-type catalysts used for other processes[17,24] (see Figure 2 and Figure 3). In each case except for structures **d** and **e** (Table 1), the formic acid···catalyst complex was found to be lower in free energy than the separated components. The computed gas-phase free energy barriers ($\Delta G^{\ddagger}$) for dehydrogenation and dehydration in Table 1 are accordingly calculated as free energy differences measured from either the formic acid···catalyst complex or the separated components, which-

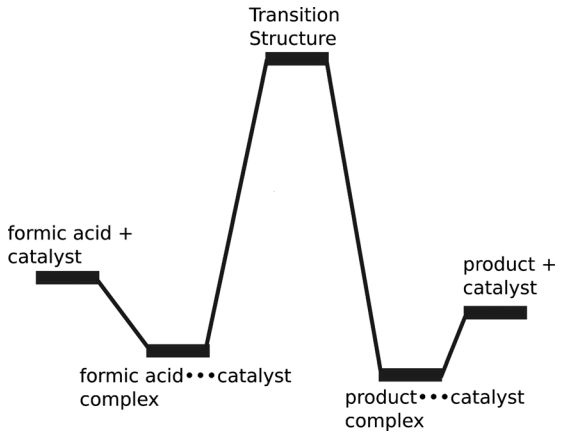

Figure 2. General potential energy profile for the decomposition of formic acid.

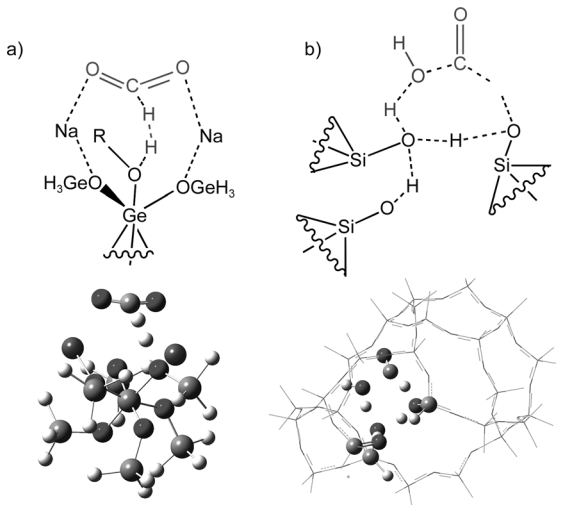

Figure 3. Calculated transition structures (TS): a) dehydrogenation TS for sodium germanate showing the involvement of sodium ions and b) dehydration TS for silicalite showing the involvement of silanol groups.

Table 1: Calculated gas-phase free energy barriers ($\Delta G^{\ddagger}$, 298 K, M06-2X/6-311+G(3df,2p)//B3-LYP/6-31+G(d,p), kJ mol^{-1}) for dehydrogenation and dehydration and energy selectivities ($\Delta\Delta G^{\ddagger}$, kJ mol^{-1}). Model catalyst structures are shown in Figure 1.

	$\Delta G^{\ddagger}$ H_2/CO_2	$\Delta G^{\ddagger}$ H_2O/CO	$\Delta\Delta G^{\ddagger}$ [a]
Uncatalyzed reaction	293.3	295.1	−1.9
Sodiated structures			
octahedral germanate (**a**)	167.2	189.6	−22.4
tetrahedral germanate (**b**)	176.8	208.9	−32.1
MFI silicalite (**f**)	190.2	263.9	−73.7
tetrahedral silicalite (**b**, Si replacing Ge)	177.8	215.8	−38.1
Protonated structures			
octahedral germanate (**c**)	158.3	163.4	−5.0
tetrahedral germanate (**d**)	204.7	223.1	−18.3
MFI germanate (**e**, Ge replacing Si)	227.6	199.8	+27.7
MFI silicalite (**e**)	220.7	133.7	+87.0

[a] A negative energy selectivity ($\Delta\Delta G^{\ddagger}$) indicates a preference, that is, lower barrier, for desirable dehydrogenation.

ever has the lower free energy (see the Supporting Information for details of all stationary points, Table S1, and Figure S2). Also included in Table 1 are the energy selectivities ($\Delta\Delta G^{\ddagger}$), defined here as the difference in the free energy barriers for dehydrogenation and dehydration. The desired preference for dehydrogenation corresponds to a negative value for $\Delta\Delta G^{\ddagger}$.

The barriers calculated for the uncatalyzed reactions are reduced by all the catalysts that we have examined (Table 1). Our computations predict that both forms of sodium germanate exhibit dehydrogenation selectivity. Specifically, the calculated energy selectivities are −22.4 kJ mol^{-1} for octahedral sodium germanate, and −32.1 kJ mol^{-1} for tetrahedral sodium germanate.

The protonated octahedral and tetrahedral germanate catalysts are also predicted to selectively dehydrogenate formic acid, though the energy selectivity is lower than that with the sodiated forms (Table 1). Thus, we would expect the germanate structure overall to be selective for dehydrogenation. However, in the case of the protonated octahedral germanate structure, very similar barriers are calculated for dehydration (163.4 kJ mol^{-1}) and dehydrogenation (158.3 kJ mol^{-1}; Table 1), suggesting that both hydrogen and water might be produced in this situation.

Protonated MFI silicalite is predicted to selectively dehydrate formic acid, as the barrier to dehydration is calculated to be 87.0 kJ mol^{-1} lower than the barrier to dehydrogenation. The analogous protonated germanate MFI structure is also predicted to predominantly lead to dehydration (Table 1), although the energy selectivity is much smaller. The selectivity of germanols (R_3GeOH groups) for dehydration (analogous to what is observed for silanols) could provide a rationalization as to why glassy germanates dehydrate formic acid.[8] It is possible that the dehydration occurs through catalysis by germanols on the glassy surface. The sodiated silicalite and sodiated MFI silicalite structures show a calculated preference for dehydrogenation (Table 1).

To explore these computational predictions experimentally, we synthesized H-silicalite-1, Na-silicalite-1, and sodium germanate by adopting literature protocols (see the Experimental Section for details). While many different geometric and molecular combinations can be easily examined theoretically, in the experimental situation only a few are available for synthesis and testing, and it has thus far not proved possible to generate a comparable H-form of the sodium germanate.

Based on X-ray diffraction (Figure 4), the sodium germanate was found to be analogous to that synthesized by Kamiya et al., who suggest that the sodium germanate crystalline state is made up of both octahedral and tetrahedral germanate units.[11] In addition, some rutile germanium(IV) oxide is present (Figure 4).[25] The synthesized silicalite-1 has an X-ray diffraction pattern (Figure S4) that can be indexed successfully according to a monoclinic MFI crystal structure.

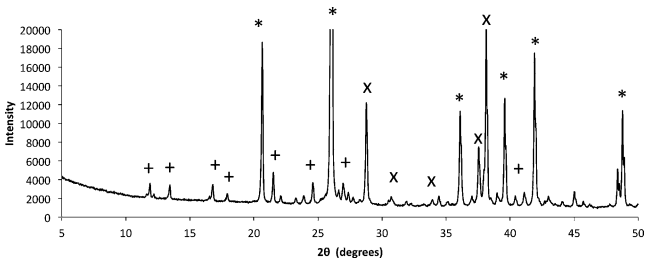

Figure 4. Measured X-ray diffraction pattern of the sodium germanate $Na_4Ge_9O_{20}$ synthesized: octahedral units (+, $Na_4Ge_9O_{20}$), tetrahedral units (×, $Na_2Ge_4O_9$), and rutile germanium (IV) oxide (*).

To determine the molar compositions of these materials, elemental analyses using ICP-AES were performed and the ratios obtained are included in Table 2. The results are consistent with the structures used in the calculations.

Table 2: Molar compositions and structural parameters for the catalysts, as determined by ICP-AES.

Catalyst	Ge	Na	Si
sodium germanate	10.0	0.95	–
H-silicalite-1	–	–	1.0
Na-silicalite-1	–	1.0	13.0

The catalytic performance of each of the sodiated and non-sodiated catalysts was evaluated by passing argon containing nominally 1 mol% formic acid vapor over the catalyst in a furnace held at 300 °C. Under these conditions, formic acid exists essentially only in the monomeric form, as modeled in the calculations. Control experiments (in the absence of catalyst) revealed minimal loss of formic acid, including over the quartz wool support used in the catalytic tests (see the Supporting Information for details). Under the test conditions, at least 50% of the formic acid is reacted, with the germanate catalyst being slightly less reactive overall. Apart from unreacted formic acid, the only products detected are CO, CO_2, and H_2. Comparing absolute concentrations, the

yield of CO_2 in the products is within 5% of that of H_2, confirming that hydrogen production occurs as described by reaction (1). Each catalyst was tested at least three times on separate dates with variations in relative product selectivity being less than 5%. Table 3 summarizes the results in terms of

Table 3: Gas components expressed as ratios and reported at steady state (after 60 min at 300°C).

Catalyst	Selectivity $H_2/(H_2+CO)$
sodium germanate	94%
H-silicalite-1	25%
Na-silicalite-1	39%

the apparent selectivity towards dehydrogenation, evaluated as the ratio, in the products, of the concentration of H_2 to the sum of the H_2 and CO concentrations. In qualitative agreement with our calculations, H-silicalite-1 preferentially performs dehydration with about 75% selectivity. However, contrary to the computational prediction, Na-silicalite-1, synthesized by ion exchange, also preferentially performs dehydration. This can be rationalized by noting that, while some sites are sodiated, aqueous workup of the samples during the catalyst synthesis tends to open up access to more defect sites, making these silanol nests (with their lower barrier for dehydration) the dominant sites for catalysis.

Our most striking result is that the synthesized sodium germanate preferentially dehydrogenates formic acid with 94% selectivity, a first for a non-transition-metal system and consistent with the predictions of our quantum chemistry calculations.

In summary, based on the computational evaluation of the hypothesis that acidity/basicity tuning should allow for selectivity inversion in formic acid decomposition, we were able to rationally design, synthesize, and test by experiment the first highly selective, non-transition-metal catalyst for formic acid dehydrogenation. The combination of computational studies as a lead generator with subsequent experimental verification has led to an important breakthrough in the field and serves to highlight the power inherent in such coupled approaches.

Experimental Section

Theoretical methods: Standard density functional theory calculations were carried out with the Gaussian 09 program.[13] Geometry optimizations for the germanates were performed with B3-LYP/6-31+G(d,p), which has been used previously with good effect for similar molecules.[17,24] Single-point energy calculations were carried out with M06-2X/6-311+G(3df,2p). For the silicalite calculations, geometry optimizations were carried out at the ONIOM(B3-LYP/6-31+G(d,p):PM6) level.[22] For the germanium MFI structure the bond lengths were increased by extending the bonds to the terminal hydrogen atoms and then reoptimizing the structure using ONIOM(B3-LYP/6-31+G(d,p):PM6) (see the Supporting Information for details). Single-point energy calculations were again carried out with M06-2X/6-311+G(3df,2p). The results of the calculations for small models are sufficient to illustrate trends in the reactivity of the germanate and silicalite catalysts but for a more fully quantitative description, larger cluster models may be necessary.

Materials: The following chemicals were used as received: Ludox AS-40 (colloidal silica, 40 wt% in water), germanium(IV) oxide (GeO_2) (99.999%) (both Sigma Aldrich), tetrapropylammonium hydroxide (TPAOH) (1M in water) (Alfa Aesar), and glacial acetic acid (99.7%) (Ajax).

Synthesis: In a typical synthesis of the germanate, 0.93 g of NaOH was dissolved in 9 mL of deionized water, then 8.4 g of GeO_2 was added and the mixture was stirred for one hour at room temperature, followed by addition of 8.2 g TPAOH (1M in water). The mixture was stirred for 1 hour at 60°C and stirred an additional hour at room temperature. A solution of 1.8 g of glacial acetic acid in 5.4 mL of deionized water was used to adjust the pH value to around 10–11 and the solution was stirred for another 10 min. The synthesis mixture was transferred to a 50 mL PTFE-lined steel autoclave and heated at 160°C for 72 h without stirring. In a typical synthesis of silicalite,[26] 12.6 g of tetraethyl orthosilicate (TEOS), 20.0 g of TPAOH (1M in water), and 0.7 g water were combined and stirred for 2 h. The mixture was transferred to an autoclave and heated at 160°C for 48 h. The contents of the autoclave (both silicalite and germanate) were centrifuged and washed three times with deionized water. The isolated material was dried at 80°C, then calcined at 300°C for 3 h, followed by 600°C for 6 h (ramp rate 1°C min^{-1}). The sodium form of the silicalite was obtained after ion exchange by washing the silicalite three times in 50 mL $NaNO_3$ solution (0.5M) at room temperature and sonicating for 5 min before separation by centrifugation and washing with deionized water each time.[27] After drying at 80°C, the sodium silicalite was calcined at 280°C for 3 h.

Characterization. Powder X-ray diffraction (XRD) measurements were made using a PANalytical X-Pert PRO MRD X-ray diffractometer equipped with a PIXcel detector, and using Ni-filtered CuK_α radiation ($\lambda_{av} = 1.5419$ Å). Initial analyses were performed using the PANalytical HighScore software. Inductively coupled plasma atomic emission spectroscopy (ICP-AES) was utilized to determine the ratios of elements in the final products.

Catalytic testing: The experimental setup (see Figure S1 in the Supporting Information) comprises a co-annular countercurrent silica flow reactor housed vertically in a temperature-controlled furnace (Lindberg/Blue M 1100°C, Moldatherm Box Furnace). Pure argon (100 sccm) regulated by a Smartrak mass flow controller (MFC) was bubbled through a 50% v/v aqueous solution of formic acid. Catalyst (150 mg) was fixed between two silica wool packages in a specific position at the lower end of the reaction tube (inside diameter 0.7 cm). In a series of blank experiments, silica wool showed minimal decomposition of formic acid up to a temperature of 300°C (see the Supporting Information for details). Two micro-GCs (Agilent micro-GC 4900) were used to sample the gaseous products at the outlet of the reactor. The GC columns used were a molecular sieve column (MS5A) for detecting hydrogen and carbon monoxide, and a Poraplot Q column (PPQ) for carbon dioxide. To protect the MS5A column from water vapor, the gaseous stream was dried by a Perma Pure Dryer (model PD 20–12 inch) before entering the GC.

Received: May 16, 2014
Published online: August 28, 2014

Keywords: dehydrogenation · formic acid · hydrogen

[1] K. E. Martin, J. P. Kopasz, K. W. McMurphy in *Fuel Cell Chemistry and Operation*, *Vol. 1040* (Eds.: A. M. Herring, T. A. Zawodzinski, Jr., S. J. Hamrock), American Chemical Society, **2010**, pp. 1–13.

[2] a) A. Alissandratos, H.-K. Kim, H. Matthews, J. E. Hennessy, A. Philbrook, C. J. Easton, *Appl. Environ. Microbiol.* **2013**, *79*, 741–

744; b) K. Schuchmann, V. Müller, *Science* **2013**, *342*, 1382 – 1385.
[3] K. Tedsree, T. Li, S. Jones, C. W. A. Chan, K. M. K. Yu, P. A. J. Bagot, E. A. Marquis, G. D. W. Smith, S. C. E. Tsang, *Nat. Nanotechnol.* **2011**, *6*, 302 – 307.
[4] S. Enthaler, *ChemSusChem* **2008**, *1*, 801 – 804.
[5] S. Enthaler, J. von Langermann, T. Schmidt, *Energy Environ. Sci.* **2010**, *3*, 1207 – 1217.
[6] A. Alissandratos, H. K. Kim, C. J. Easton, *Bioresour. Technol.* **2014**, *164*, 7 – 11.
[7] W. L. Nelson, C. J. Engelder, *J. Phys. Chem.* **1926**, *30*, 470 – 475.
[8] N. Yoshida, K. Miyataka, S. Kishimoto, *J. Catal.* **1984**, *88*, 237 – 239.
[9] L. K. Freidlin, A. M. Levit, *Zh. Obshch. Khim.* **1951**, *21*, 1255 – 1264.
[10] M. Ai, *J. Catal.* **1977**, *50*, 291 – 300.
[11] K. Kamiya, M. Tatsumi, J. Matsuoka, H. Nasu, *Phys. Chem. Glasses* **1998**, *39*, 9 – 16.
[12] Y. Zhao, D. G. Truhlar, *Theor. Chem. Acc.* **2008**, *120*, 215 – 241.
[13] M. J. Frisch, et al. Gaussian, Inc., Wallingford CT, **2009**.
[14] E. M. Flanigen, J. M. Bennett, R. W. Grose, J. P. Cohen, R. L. Patton, R. M. Kirchner, J. V. Smith, *Nature* **1978**, *271*, 512 – 516.
[15] H. Kosslick, V. A. Tuan, R. Fricke, C. Peuker, *Ber. Bunsen-Ges.* **1992**, *96*, 1761 – 1765.
[16] See for example: a) J. Van der Mynsbrugge, J. De Ridder, K. Hemelsoet, M. Waroquier, V. Van Speybroeck, *Chem. Eur. J.* **2013**, *19*, 11568 – 11576; b) V. Van Speybroeck, J. Van der Mynsbrugge, M. Vandichel, K. Hemelsoet, D. Lesthaeghe, A. Ghysels, G. B. Marin, M. Waroquier, *J. Am. Chem. Soc.* **2011**, *133*, 888 – 899.
[17] B. Chan, L. Radom, *J. Am. Chem. Soc.* **2008**, *130*, 9790 – 9799.
[18] The MFI crystal structure was obtained from the Inorganic Crystal Structure Database (ICSD) and was originally published in D. H. Olsen, G. T. Kokotailo, S. L. Lawton, W. M. Meier, *Nature* **1978**, *271*, 512 – 516.
[19] J. Sauer, A. Bleiber, *Catal. Today* **1988**, *3*, 485 – 492.
[20] J. Sauer, W. Schirmer, *Stud. Surf. Sci. Catal.* **1988**, *37*, 323 – 332.
[21] T. Kobayashi, J. A. DiVerdi, G. E. Maciel, *J. Phys. Chem. C* **2008**, *112*, 4315 – 4326.
[22] See for example: a) S. Dapprich, I. Komiromi, K. S. Buyn, K. Morokuma, M. J. Frisch, *THEOCHEM* **1999**, *461 – 462*, 1; b) T. Vreven, K. S. Byun, I. Komaromi, S. Dapprich, J. A. Montgomery, Jr., K. Morokuma, M. J. Frisch, *J. Chem. Theory Comput.* **2006**, *2*, 815 – 826.
[23] A. P. Scott, L. Radom, *J. Phys. Chem.* **1996**, *100*, 16502 – 16513.
[24] S. Senger, L. Radom, *J. Am. Chem. Soc.* **2000**, *122*, 2613 – 2620.
[25] A. A. Bolzan, C. Fong, B. J. Kennedy, C. J. Howard, *Acta Crystallogr. Sect. B* **1997**, *53*, 373 – 380.
[26] S. P. B. Kremer, C. E. A. Kirschhock, A. Aerts, K. Villani, J. A. Martens, O. I. Lebedev, T. G. Van, *Adv. Mater.* **2003**, *15*, 1705 – 1707.
[27] A. Ghosh, V. N. Garcia, S. F. Mitchell, S. Stevenson, D. F. Shantz, *J. Phys. Chem. C* **2009**, *113*, 12252 – 12259.

